View metadata, citation and similar papers at core.ac.uk
brought to you by CORE
provided by CiteSeerX

Controlling spatiotemporal dynamics of flame fronts

Valery Petrov and Michael F. Crowley
Department of Chemistry, West Virginia University, Morgantown, West Virginia 26506-6045

Kenneth Showalter
Department of Chemistry, West Virginia University, Morgantown, West Virginia 26506-6045 and Service de Chimie Physique, Université Libre de Bruxelles, Campus Plaine, 1050 Bruxelles, Belgium

(Received 22 June 1994; accepted 1 July 1994)

In certain mixtures of fuel and oxidizer, propagating flame fronts may exhibit both stable and unstable cellular structures. Such flames represent spatially extended chemical systems, with coupling from diffusion of heat and reactants. A new algorithm is proposed that allows the stabilization and tracking of a steady, two-cell front through a bifurcation sequence that eventually leads to chaotic behavior. Periodic modes of the front can also be stabilized and tracked. The system is stabilized by monitoring one experimentally accessible variable and perturbing one boundary condition. No knowledge of the detailed dynamics of the system (i.e., the underlying governing equations) is required to implement the tracking method. The algorithm automatically provides information about the locations of the unstable steady states and periodic orbits and the magnitudes of the associated eigenvalues and Floquet multipliers.

I. INTRODUCTION

When a mixture of fuel and oxidizer is ignited, a wave of exothermic chemical reaction propagates through the mixture, producing heat and converting initial reactants into products. The planar front of a premixed flame, propagating through an initially motionless and homogeneous reaction mixture, may become unstable under certain conditions.[1–3] Two different types of instabilities arise: the hydrodynamic flame instability and the thermo-diffusive flame instability.[4] Hydrodynamic instabilities are caused by changes in density due to thermal expansion of the burned gas and are always present in large-scale flames. Thermo-diffusive instabilities arise from small-scale perturbations and depend on the presence of a reactant component with a sufficiently high molecular diffusivity.

We present an algorithm that can be used to stabilize steady flame fronts, suppressing the natural oscillatory behavior. It can also be used to stabilize periodic oscillations of the front that would otherwise be unstable. The algorithm utilizes a map-based tracking scheme that allows adaptive control of the system under slowly varying conditions.[5] To demonstrate the method we focus on the thermo-diffusive instability, neglecting the effects of thermal expansion by assuming the density of the gaseous mixture is everywhere constant.

In the thermo-diffusive instability, the flame front becomes nonplanar at a critical value of a system parameter such as the Lewis number. On further changing the parameter, the cellular front loses its stability to display spatiotemporal oscillations. The emergence of a period-doubling cascade in the two-cell front—and the control of such fronts—is the focus of this investigation. We study the control of two-dimensional premixed flames with a standard partial differential equation (PDE) model and a one-variable reduction of this model given by the Kuramoto–Sivashinsky equation. A description of the dynamical behavior of each system by a one-dimensional map allows the application of the tracking algorithm.

Several recent studies have reported control and tracking of unstable steady states in dynamical systems with many degrees of freedom. Gills *et al.*[6] reported tracking steady states in a chaotic multimode laser, thereby extending the range of stable lasing beyond that of the autonomous system. Unstable steady states and periodic orbits were tracked in a similar laser system by Glorieux and co-workers.[7] Hjelmfelt and Ross[8] stabilized and tracked unstable stationary states in a spatially extended chemical system with a linear feedback method that relies on a model description. We recently used a model-independent method to track unstable periodic orbits in the Belousov–Zhabotinsky (BZ) reaction in both the chaotic and complex-periodic parameter ranges.[5] The adaptive tracking algorithm is an extension of a map-based control method[9,10] that was previously used to control chaos in the BZ reaction.[11] The map-based scheme is a reduction of the Ott–Grebogi–Yorke (OGY) algorithm.[12,13]

The tracking algorithm is modified in this study to stabilize steady states and periodic orbits in spatiotemporal flame systems. In Sec. II, we describe the model systems and discuss some features of the calculations. We show how the behavior of a system near a focus-type steady state can be described by a one-dimensional map in Sec. III. Stabilizing and tracking unstable steady states and periodic orbits in the Kuramoto–Sivashinsky system and in the full PDE system are described in Secs. IV and V. We conclude in Sec. VI by describing potential applications of the method.

II. MODEL SYSTEMS

A. Reaction–diffusion model

Premixed flames with thermo-diffusive instabilities can be described by a system of two partial differential equations, one for temperature and the other for the concentration of a stoichiometrically deficient reactant:

 0021-9606/94/101(8)/6606/9/$6.00 © 1994 American Institute of Physics

Downloaded 09 Jul 2002 to 141.14.151.181. Redistribution subject to AIP license or copyright, see http://ojps.aip.org/jcpo/jcpcr.jsp

$$\rho c_p \frac{\partial T}{\partial t} = \kappa \nabla^2 T + qW, \tag{1}$$

$$\frac{\partial C}{\partial t} = D_c \nabla^2 C - W. \tag{2}$$

Here, T is the temperature of the gaseous mixture, C is the concentration of the stoichiometrically deficient component, ρ is the density, c_p is the specific heat, κ is the thermal conductivity of the mixture, $\nabla^2 = \partial^2/\partial X^2 + \partial^2/\partial Y^2$ is the 2-D Laplacian operator, q is the heat release of the reaction, and D_c is the diffusion coefficient for the reactant C. The temperature dependence of the rate of chemical reaction W is given by an Arrhenius equation,

$$W = KC \exp(-E/RT), \tag{3}$$

where E is the activation energy, R is the universal gas constant, and the constant K includes the frequency factor and the concentration of the reactant in stoichiometric excess. The reaction zone is taken to be infinite in extent in the X coordinate ($-\infty < X < +\infty$) but of finite width L in the Y coordinate ($0 \leq Y \leq L$). We assume zero-flux boundary conditions at $Y = 0$ and L.

For convenience, we transform (1) and (2) into the dimensionless equations

$$\frac{\partial \theta}{\partial \tau} = \nabla^2 \theta + (1-\epsilon)\omega, \tag{4}$$

$$\frac{\partial s}{\partial \tau} = (1/\mathscr{L})\nabla^2 s - \omega, \tag{5}$$

where $\theta = T/T_b$ is the dimensionless temperature scaled by the final temperature T_b behind the front ($T_b = T_0 + qC_0/c_p\rho$, with T_0 the ambient temperature) and $\epsilon = T_0/T_b$; $s = C/C_0$ is the dimensionless concentration scaled by the concentration of reactant C_0 ahead of the front; $\tau = Kt$, $x = (K\rho c_p/\kappa)^{1/2} X$ and $y = (K\rho c_p/\kappa)^{1/2} Y$ are dimensionless time and spatial coordinates; $\omega = s \exp(-N/\theta)$ is the dimensionless reaction rate with $N = E/RT_b$; and $\mathscr{L} = \kappa/\rho c_p D_c$ is the Lewis number. The boundary conditions appropriate for the propagating front are

$$\begin{aligned} &s = 1, \quad \theta = \epsilon \text{ as } x \to +\infty; \\ &s = 0, \quad \theta = 1 \text{ as } x \to -\infty, \end{aligned} \tag{6}$$

where the front is moving in the positive x direction. The zero-flux boundary conditions in the y coordinate are

$$\frac{\partial s}{\partial y} = \frac{\partial \theta}{\partial y} = 0 \quad \text{at } y = 0 \text{ and } L. \tag{7}$$

It is convenient to introduce a traveling coordinate system in the x direction with a speed of the flame front v. This transformation adds a new term, $v\,\partial/\partial x$, to Eqs. (4) and (5):

$$\frac{\partial \theta}{\partial \tau} = \nabla^2 \theta + v\frac{\partial \theta}{\partial x} + (1-\epsilon)\omega, \tag{8}$$

$$\frac{\partial s}{\partial \tau} = (1/\mathscr{L})\nabla^2 s + v\frac{\partial s}{\partial x} - \omega. \tag{9}$$

The 1-D solution of Eqs. (8) and (9), calculated using finite differences for the $\partial/\partial x$ and $\nabla^2 = \partial^2/\partial x^2$ operators, is shown in Fig. 1. The limits of the grid in the x direction were set to cutoff values in order to carry out the integration. The boundary conditions become

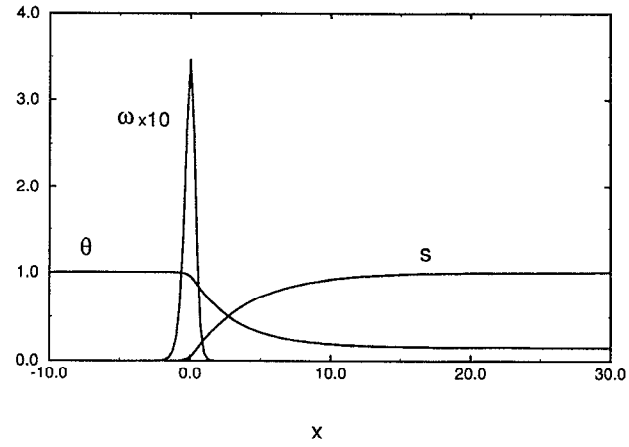

FIG. 1. Profiles of concentration s, temperature θ, and reaction rate ω in the 1-D propagating flame front. To visualize the profiles, the rate ω was rescaled by a factor of 10 and the dimensionless time and space coordinates were rescaled by setting the reaction rate $\omega = 10^{10}\, s \exp(-20/\theta)$ [which rescales time by a factor of 10^{10} and space by a factor of $(10^{10})^{1/2}$]. The asymptotic velocity of the front is 0.322; $\mathscr{L} = 0.8$, $\epsilon = 0.15$, $N = 20$.

$$\begin{aligned} &s = 1, \quad \theta = \epsilon \quad \text{at } x = x^+; \\ &s = 0, \quad \theta = 1 \quad \text{at } x = x^-, \end{aligned} \tag{10}$$

where the front is positioned near $x = 0$, and x^+ and x^- are the positive and negative cutoff coordinates. The steepness of the rate profile $\omega(x)$, which is due to the highly nonlinear Arrhenius temperature dependence, imposes a limit on the maximum value of the grid cell size. Both the grid cell size and the cutoff coordinates were varied to determine appropriate values for the study, where the front behavior is independent of the particular values chosen.

The 2-D solution was calculated using an operator splitting method,[14] a two-step technique with implicit integration of reaction and diffusion terms in the x direction and explicit integration of diffusion terms in the y direction. Four iterations were typically required in each step of the integration for convergence, where the solution was effectively unchanged with further iterations. The operator splitting method was found to be three times faster than a standard implicit algorithm, which required the solution of large sparse matrices.

The 1-D wave profile shown in Fig. 1 is also a valid solution to the 2-D system, subject to the boundary conditions (6) and (7). Thus, steady planar fronts propagating in the x direction would be anticipated for the 2-D system. For certain experimental conditions, however, such planar flames become unstable, producing cellular structures that are either stationary or undergo periodic or chaotic motions.[3] These instabilities usually occur in mixtures containing relatively light reactants that are stoichiometrically deficient, e.g., lean hydrogen–oxygen flames. Instabilities may also occur in rich hydrocarbon flames if light, mobile chain carriers such as H-atoms are produced. The system described by Eqs. (8) and

Downloaded 09 Jul 2002 to 141.14.151.181. Redistribution subject to AIP license or copyright, see http://ojps.aip.org/jcpo/jcpcr.jsp

(9) exhibits instabilities similar to those observed in real flames over a range of parameter values. However, because the numerical integration of the PDE model is computationally intensive, calculations were also carried out using the reduced model described below.

B. The Kuramoto–Sivashinsky equation

The 2-D system described by Eqs. (8) and (9) can be reduced to a single equation by assuming that reaction takes place in an infinitely narrow zone. A stability analysis of the PDEs shows that the (infinitely narrow) front becomes unstable when the diffusion of the fuel dominates over the heat conductance.[15] The condition for instability in terms of the Lewis number is given by

$$\mathscr{L}<1-2/N(1-\epsilon). \tag{11}$$

The reduction of Eqs. (8) and (9) to a single equation was developed by Sivashinsky[16] and Kuramoto.[17] The Kuramoto–Sivashinsky equation gives the temporal evolution of the front as a function of its spatial derivatives,

$$\frac{\partial \Psi}{\partial t}=\left(\frac{\partial \Psi}{\partial y}\right)^2-\frac{\partial^2 \Psi}{\partial y^2}-\frac{\partial^4 \Psi}{\partial y^4}, \tag{12}$$

with the dependent variable $\Psi(y,t)$ representing the contour of the front. The evolution equation, as it is written here, already satisfies the condition for the onset of instability. The only bifurcation parameter is the width of the reaction zone in the y direction.

An unusually rich sequence of bifurcations is exhibited by Eq. (12) as the width of the reaction zone is increased.[18] With no-flux boundary conditions, single- and multiple-cell structures are exhibited, each displaying spatiotemporal behavior ranging from steady to chaotic. We focus on the two-cell structure observed over the range $16.5 \leqslant L \leqslant 18.5$ of the reaction zone width. Profiles of the front for three different values of L are shown in Fig. 2. The relative position of the local minimum in the profile serves as a convenient observable and its time trace is also plotted for each value of L. Figure 2(a) shows the steady front for $L=16.5$ with a symmetrical two-cell structure. This front shows no temporal variation. At $L=16.8$, the steady two-cell front loses stability through a Hopf bifurcation and begins to oscillate. A snapshot of the oscillatory front and the time trace of the local minimum are shown in Fig. 2(b) for $L=17.5$. Simple oscillations are exhibited at this reaction width. As the width is increased, a series of period doubling bifurcations leads to chaotic behavior, which appears at $L=18.1$. The front profile and the chaotic time series of the local minimum are shown in Fig. 2(c) for $L=18.3$. At $L=18.33$, the strange attractor is destroyed and randomly moving traveling waves in the profile are exhibited. The control method described in the next section allows suppression of the front oscillations over the entire range of L where the two-cell structure is observed.

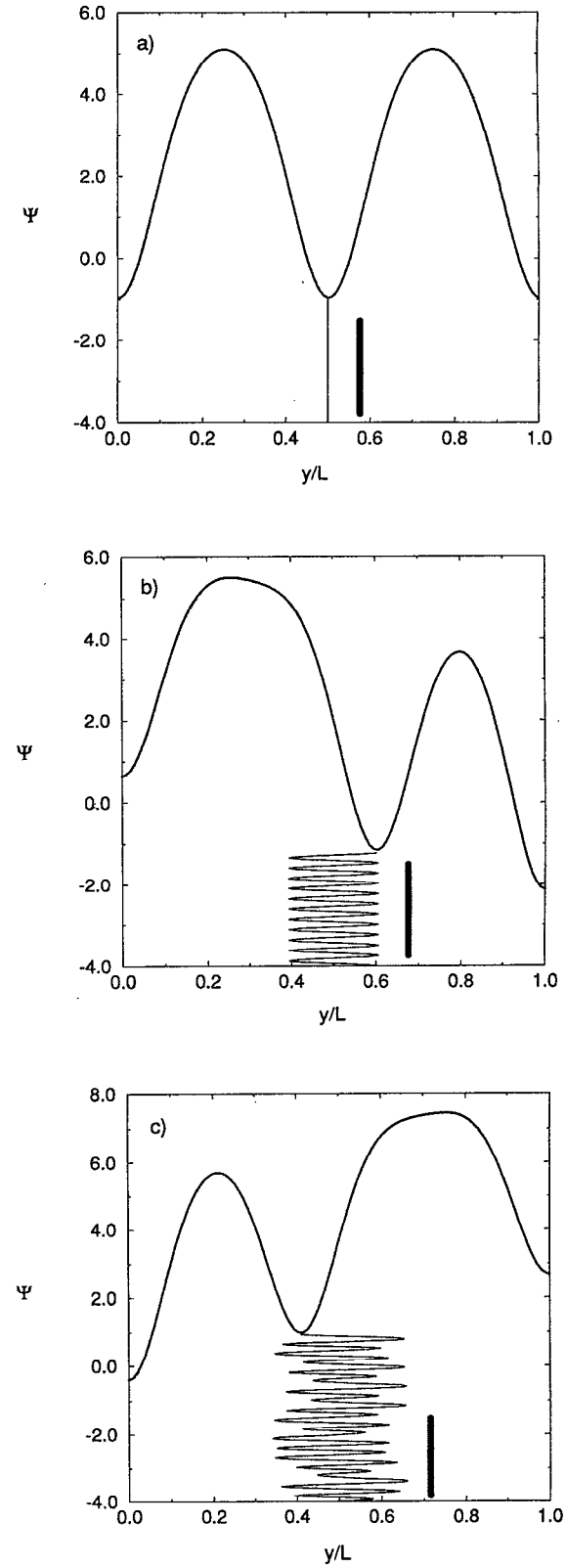

FIG. 2. Solution of the Kuramoto–Sivashinsky equation with no-flux boundary conditions showing steady (a), periodic (b), and chaotic (c) two-cell fronts for $L=16.5$, 17.5, and 18.3. The relative position of the local minimum in the profile is used to monitor the temporal evolution of the front. The time series in each figure shows the spatiotemporal motion of the minimum, with the vertical bar representing 100.0 dimensionless time units.

III. STABILIZATION AND TRACKING ALGORITHM

A. Stabilization of the steady state

The stabilization algorithm takes advantage of the linear evolution of a system in the proximity of a steady state. (The

Downloaded 09 Jul 2002 to 141.14.151.181. Redistribution subject to AIP license or copyright, see http://ojps.aip.org/jcpo/jcpcr.jsp

stabilization of periodic orbits is discussed below in Sec. IV.) For an unstable focus, oscillations initially grow in a plane defined by the unstable manifold. In the local vicinity of the steady state, the system can therefore be treated as two-dimensional since trajectories are attracted to and remain in this plane. (We assume that all other manifolds of the steady state are stable.) We assign the variables ξ_1 and ξ_2 to the plane and describe the state of the system by the vector $\bar{\xi}$, with the focus steady state at $\bar{\xi}_F$:

$$\bar{\xi}=\begin{pmatrix}\xi_1\\ \xi_2\end{pmatrix}, \quad \bar{\xi}_F=\begin{pmatrix}0\\ 0\end{pmatrix}. \tag{13}$$

The evolution near the steady state is governed by the system of linear equations

$$\frac{\partial\bar{\xi}}{\partial t}=\mathbf{A}\bar{\xi}, \tag{14}$$

where $\mathbf{A}$ is a 2×2 matrix with a pair of complex-conjugate eigenvalues, $\alpha\pm i\omega$, giving solutions of the form

$$\bar{\xi}(t)=e^{\alpha t}[\bar{b}_1\sin(\omega t)+\bar{b}_2\cos(\omega t)]. \tag{15}$$

The experimentally observable variable, $Y(t)$, is some projection of $\bar{\xi}$. The measured motion of the system will therefore have the form

$$Y(t)=e^{\alpha t}C_1\sin(\omega t+\theta)+Y_F, \tag{16}$$

for some C_1 and θ, with the observed focus at Y_F. We define $y(t)=Y(t)-Y_F$ and $\theta=0$, giving

$$y(t)=e^{\alpha t}C_1\sin(\omega t). \tag{17}$$

For $\alpha>0$, the system will spiral away from the focus with the exponential growth of $y(t)$ modulated by sinusoidal oscillations. It is natural to monitor the growing oscillations by measuring the maximum or minimum of $y(t)$. From the time derivative of (17),

$$\frac{\partial y(t)}{\partial t}=e^{\alpha t}C_2\sin(\omega t+\theta_1), \tag{18}$$

we see that the extrema of $y(t)$ are equally spaced in time by $\Delta t=\pi/\omega$. The appearance of the maxima and minima is therefore subject to the recursion relation

$$y_{i+1}=\eta y_i, \tag{19}$$

where y_i and y_{i+1} are the successive values and $\eta=-\exp(\alpha\pi/\omega)$.

The trajectory of a two-variable, linear system is shown in Fig. 3, where the horizontal axis represents the measured variable $y(t)$. Note that the extrema of $y(t)$ occur when the trajectory crosses axis M in the ξ plane. We assume that some system parameter p is used for control and that variation of this parameter causes a shift of the steady state $\bar{\xi}_F$ along line P in the ξ plane.

The steady state is stabilized by temporarily shifting its position in phase space such that the resulting trajectory (around the shifted steady state) passes through the position of the unperturbed steady state. When the system reaches this point along the trajectory, the perturbation is removed. In the targeting procedure used here, the perturbation is applied when the trajectory intersects P and is removed a half period later. The steady state is shifted to a point, indicated in Fig. 3 by a square, around which the perturbed system evolves to target the unperturbed steady state.

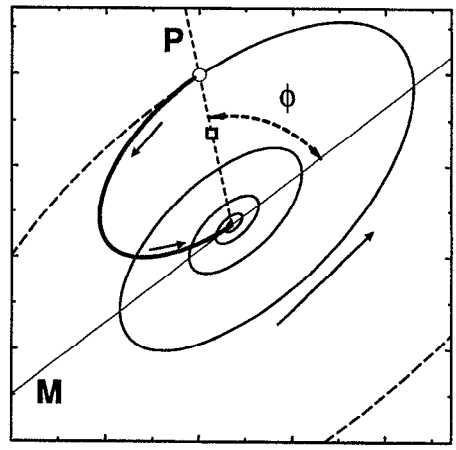

FIG. 3. The trajectory of a linear two-variable system near the stationary state. ϕ is the phase difference between the appearance of the maximum in $y(t)$ (at line M) and the direction of the steady state shift (along line P). The bold curve shows the trajectory that targets the steady state when the perturbation is applied.

As shown in Fig. 3, the perturbation must be applied at a phase ϕ following the appearance of the maximum in the measured variable $y(t)$. To synchronize the perturbation with the detection of the extremum, another variable, $z(t)$, is introduced:

$$z(t)=y(t)\left[\cos(\phi)+\frac{\alpha}{\omega}\sin(\phi)\right]-\frac{\partial y(t)}{\partial t}\frac{1}{\omega}\sin(\phi). \tag{20}$$

It follows from (17) and (20) that

$$z(t)=e^{\alpha t}C_1\sin(\omega t-\phi). \tag{21}$$

Therefore, $z(t)$ has the necessary phase shift with respect to $y(t)$. The value of ϕ can be determined by perturbing the steady state when the system is at $\bar{\xi}_F$. The trajectory will spiral out from the shifted steady state, reaching its extrema in $y(t)$ at times $(n\pi-\phi)/\omega$ after the perturbation.

Using the experimentally determined value of ϕ with Eq. (20), perturbations are applied and removed at the extrema of the new variable $z(t)$, which occur at the same phase of oscillation for all shifts of the steady state along P. The appearance of the extrema of $z(t)$ is also governed by Eq. (18) and the recursion relation (19). The effect of the perturbation Δp is given by[5]

$$z_{i+1}=\eta z_i+(1-\eta)\frac{\partial z_F}{\partial p}\Delta p. \tag{22}$$

When the perturbation is proportional to z_i,

$$\Delta p=Kz_i, \tag{23}$$

the steady state is targeted if

$$K=K_0=\frac{\eta}{(\eta-1)(\partial z_F/\partial p)}. \tag{24}$$

Downloaded 09 Jul 2002 to 141.14.151.181. Redistribution subject to AIP license or copyright, see http://ojps.aip.org/jcpo/jcpcr.jsp

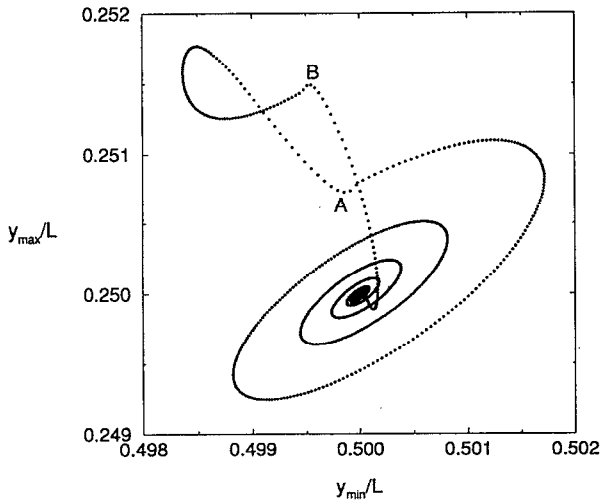

FIG. 4. Phase portrait showing a trajectory calculated from Eq. (12) at $L=17.5$ during a targeting perturbation. The horizontal axis represents the position of the local minimum in the profile relative to the width of the reaction zone. The vertical axis represents the relative position of one of the neighboring local maxima in the profile. A perturbation imposed at point A and removed at point B shifts the steady state off the unstable manifold of the stationary state. The stationary state is accurately targeted, however, because the perturbation-free period allows the system to relax along the stable manifold.

In multidimensional systems such as the Kuramoto–Sivashinsky equation, the stable manifolds may play an important role in the control algorithm. Figure 4 shows a typical trajectory arising from the application of the algorithm to Eq. (12). The system initially spirals out from the unstable focus. The perturbation was applied at point A and removed at point B. The resulting trajectory shows that although the steady state is shifted out of the plane of the unstable manifold, the focus is targeted after the perturbation is removed at point B. For accurate targeting, the system must have sufficient time to relax to the plane of the unstable focus after the perturbation is removed; otherwise, the next perturbation will be erroneously determined according to the system state at some position between point B and the steady state. The algorithm is therefore implemented with a perturbation-free period to allow the system to relax. The perturbation is applied for half the period according to Eq. (23) when the extremum in $z(t)$ is observed. It is removed for the next half period, letting the system relax along the stable manifold. The procedure is then repeated. In applying this technique to Eq. (12), the perturbations become very small (effectively approaching zero) as the system converges to the steady state. The targeting procedure therefore changes only the stability of the steady state and not its position. It should be noted that essentially the same delay technique was first used by Hunt[19] to stabilize high-periodicity orbits in a driven diode system. It has since been used in a number of studies, including controlling chaos in a laser[20] and in the Belousov–Zhabotinsky reaction.[11] Other means of targeting that do not rely on a perturbation-free period have been proposed, including a recursive proportional feedback method by Rollins, Parmananda, and Sherard[21] and a multiparameter scheme by Petrov, Peng, and Showalter.[10]

B. Stability analysis and tracking

A stability analysis subroutine is used to interrogate the steady state. The stability of the steady state under control can be changed by varying the proportionality constant K, and the response of the system to a sequence of variations yields the stability of the autonomous steady state.[5] For an arbitrary K, Eqs. (22) and (23) can be rewritten as

$$z_{i+1}=Sz_i. \tag{25}$$

The slope S, which depends linearly on the proportionality constant K, defines the stability of the system under control:

$$S=\lambda+\frac{\partial z_F^*}{\partial p}K(1-\lambda), \tag{26}$$

where $\lambda=\eta^2=\exp(2\pi\alpha/\omega)$ and

$$\frac{\partial z_F^*}{\partial p}=\frac{\partial z_F}{\partial p}\frac{\eta}{1+\eta}. \tag{27}$$

With the incorporation of a delay period to allow the system to relax between perturbations, z_F^* is the effective shift of the fixed point over the full period of oscillation for a perturbation applied over half the period. The behavior of the system under control can therefore be described in terms of the z_{i+1} vs z_i map. The ability to change the slope S of the map by an appropriate choice of K is an integral feature of the tracking algorithm.[5]

In each step of the tracking, the proportionality constant K is set to a value, K_1, that will produce a slightly unstable steady state. As the system diverges away from the steady state, points are collected for an accurate determination of the slope S_1. Before the system has evolved beyond the linear control range, K is changed to a new value, K_2, which corresponds to a mildly stable steady state. As the system converges to the steady state, values are again collected for an accurate determination of the corresponding slope S_2. The proportionality constants and corresponding slopes are then used to calculate K_0, the proportionality constant that produces a map of zero slope under control, and λ, the slope of the map of the autonomous system:[5]

$$K_0=\frac{S_2K_1-S_1K_2}{S_2-S_1} \tag{28}$$

and

$$\lambda=\frac{S_2K_1-S_1K_2}{K_1-K_2}. \tag{29}$$

The steady state becomes super-stable when the proportionality constant K_0 is used in the control algorithm. With each increment of the bifurcation parameter, the steady state is stabilized by repeating the stability analysis.

Downloaded 09 Jul 2002 to 141.14.151.181. Redistribution subject to AIP license or copyright, see http://ojps.aip.org/jcpo/jcpcr.jsp

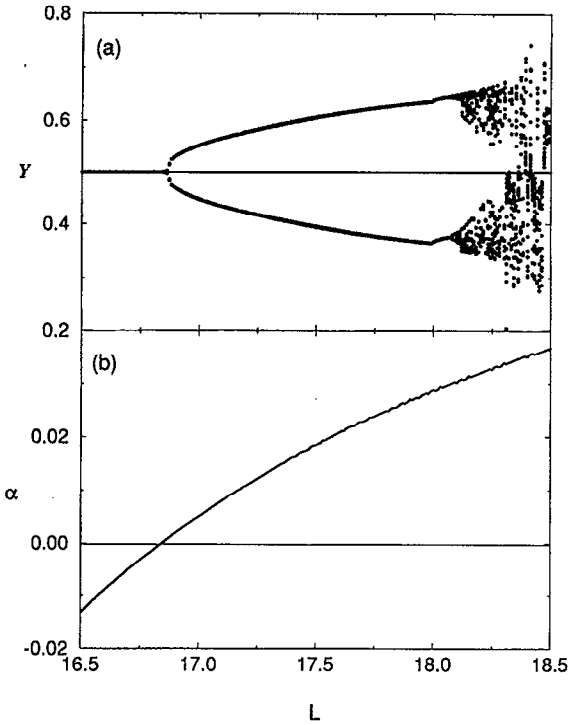

FIG. 5. (a) Bifurcation diagram of the autonomous system and the stabilized steady front calculated from the Kuramoto–Sivashinsky equation. Solid points give the relative maximum and minimum of oscillation of $Y=(y_{min}/L)$ as a function of the bifurcation parameter L. The position of the stabilized steady front is shown by the solid line. (b) Value of the real part of the complex conjugate eigenvalues as a function of L.

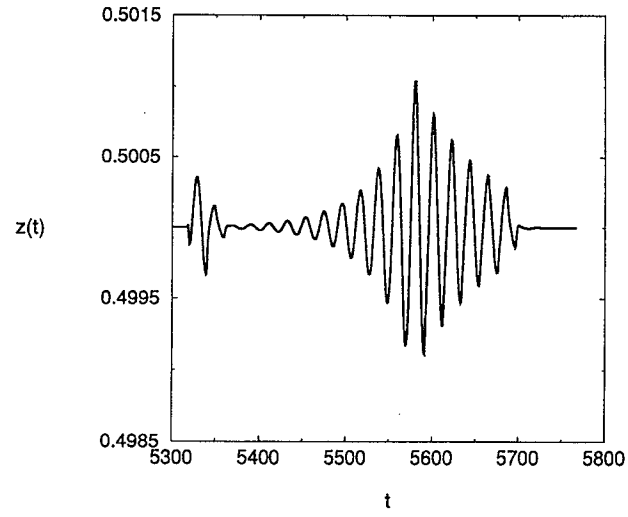

FIG. 6. Time series showing one step of the tracking procedure at $L=17.5$. A perturbation is first applied to determine ϕ. The following series of oscillations with increasing and decreasing amplitude is used to determine the stability of the steady state (see text).

IV. TRACKING STEADY AND PERIODIC FRONTS IN THE KURAMOTO–SIVASHINSKY SYSTEM

The unstable states of the Kuramoto–Sivashinsky equation provide an interesting testing ground for the tracking algorithm. We first demonstrate the method by stabilizing the steady two-cell front through the period-doubling and chaotic ranges of the bifurcation parameter L. We then demonstrate the tracking of periodic orbits by stabilizing period-one oscillations through the same range. The position of the local minimum in the front profile was utilized as the "experimental" observable for the tracking procedure. It is a convenient choice because the steady solution is symmetrical for all L, with the minimum exactly at the center of the reaction zone.

The bifurcation diagram of the autonomous system is shown in Fig. 5(a). The solution is stable for $L<16.8$, with the position of the minimum in the front profile, $Y=y_{min}/L$, remaining at the center of the reaction zone [cf. Fig. 2(a)]. A Hopf bifurcation occurs at $L=16.85$, and the front begins to oscillate. The solid circles show the maximum and minimum of the oscillations [cf. Fig. 2(b)]. As the width is increased, a symmetry-breaking bifurcation occurs at $L=18.0$ and two mirror-image, period-one solutions appear, each of which exhibit oscillations centered above or below the middle of the reaction zone. The symmetry-breaking bifurcation is necessary for this symmetrical system to develop a series of period-doubling bifurcations leading to a chaotic attractor.[22] (For clarity, only one of the solutions is shown in the bifurcation diagram.) As the width is increased, the oscillations become more complex through the period-doubling cascade to eventually become chaotic at $L=18.1$ [cf. Fig. 2(c)]. At $L=18.33$, the oscillatory chaos disappears and more complex behavior is exhibited, where minima in the front profile randomly appear only to coalesce with other minima and the system boundaries.

The steady flame front is stabilized by varying the boundary conditions to simulate perturbations to the fuel supply. The no-flux boundary condition, $\partial\Psi/\partial y=0$ in Eq. (12), was varied according to z_i in Eq. (23) at one boundary. This control parameter corresponds to an experimental setting in which there are minute, asymmetric variations in the fuel supply. Since the system is symmetrical at the steady state, an asymmetric perturbation is necessary to affect the steady state position.

Figure 6 shows a time series during one step of the tracking algorithm as the width of the reaction zone was changed from $L=17.4$ to 17.5. A perturbation was first applied at $t=5318$ to calculate the phase ϕ of the projected oscillations. This is used in Eq. (20) to transform to the variable $z(t)$. The proportionality constant was then set to the value $K_1=-24.2$ at $t=5360$ to produce a slightly unstable state. The resulting oscillations gradually increase in amplitude, as shown in Fig. 6. At $t=5580$, the proportionality constant is changed to a new value, $K_2=178.9$, which corresponds to a mildly stable state. Figure 6 shows these oscillations gradually decreasing in amplitude. The local slopes S_1 and S_2 corresponding to K_1 and K_2 are determined from the z_{i+1} vs z_i return maps. Figure 7 shows the maps for the diverging and converging system. The values of K_1, K_2, S_1, and S_2 allow the determination of K_0 from Eq. (28). The steady state is then targeted using the updated K_0, shown in Fig. 6 at $t=5685$.

Due to the symmetry of the two-cell front (and the choice of the local minimum in the profile as the monitored

Downloaded 09 Jul 2002 to 141.14.151.181. Redistribution subject to AIP license or copyright, see http://ojps.aip.org/jcpo/jcpcr.jsp

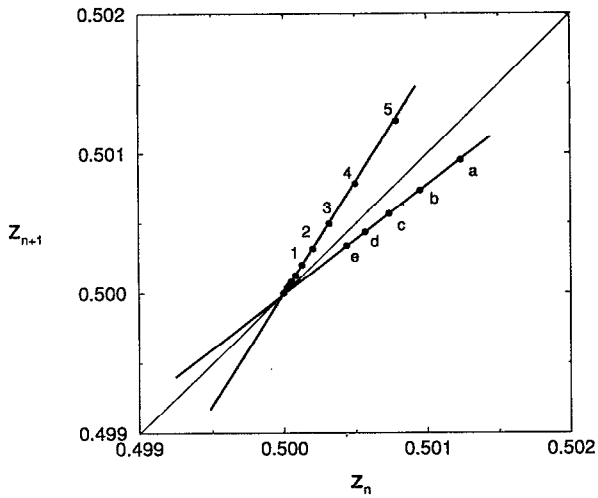

FIG. 7. Return maps for the tracking step in Fig. 6. Two different values of K cause the system to diverge away from the stationary state (1,2,3,...) and converge back to that state (a,b,c,...). The proportionality constant was first set to $K_1=-24.2$ and then to $K_2=178.9$ to generate the divergent and convergent behavior. The corresponding values of S_1 and S_2 in Eqs. (28) and (29) yield the values $K_0=373.7$ and $\lambda=1.48$.

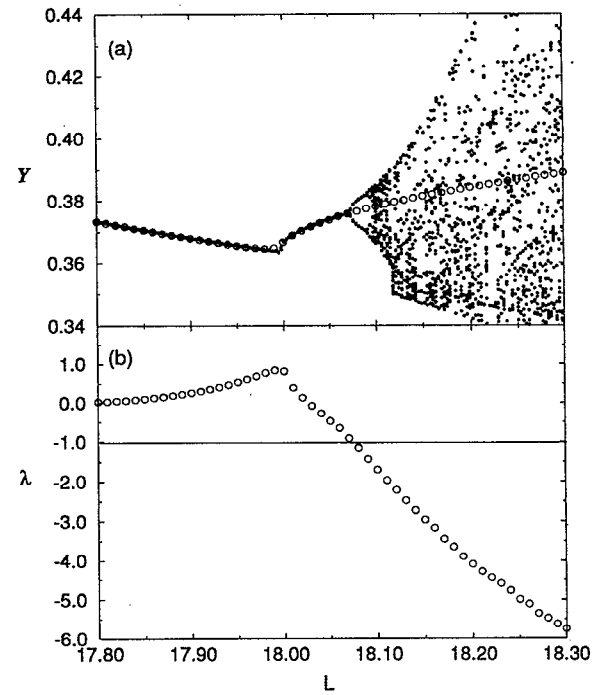

FIG. 8. Stabilization and tracking of period-1 oscillations. (a) Bifurcation diagram calculated from Eq. (12), where the solid points represent the oscillation minimum of the local minimum in the front profile, $Y=(y_{min}/L)_{min}$. The open circles show the locus of the tracked period-1 orbit. (b) Value of the period-1 Floquet multiplier as a function of L.

variable), the position of the steady state remains at $Y=y_{min}/L=0.5$. The steady state position therefore does not require reevaluation by the tracking procedure when the bifurcation parameter is changed. The solid line in Fig. 5(a) shows the stabilized front at $Y=0.5$ following the Hopf bifurcation at $L=16.85$. The steady-state stability of the autonomous system is also determined by the tracking algorithm. Figure 5(b) shows the real part of the complex conjugate eigenvalues of the focus plotted as a function of the reaction zone width. Both stable and unstable steady states can be examined, since the appropriate choice of K causes the system to either converge to or diverge from the steady state, thereby allowing the eigenvalues to be determined from Eq. (29).

The tracking algorithm can also be used to stabilize periodic oscillations of the front. For periodic orbits, the algorithm relies on the saddle character of the corresponding fixed points in the Poincaré section. As previously reported, periodic orbits with only one unstable manifold and highly attractive stable manifolds can be readily stabilized and tracked.[5] The method is analogous to that for stabilizing steady states except no phase correction is necessary. The oscillatory behavior of Eq. (12) is described according to a 1-D map by plotting the current minimum of oscillation with respect to the previous minimum. The period-1 orbit is then stabilized and tracked by targeting the fixed point in the map. As in earlier applications,[5,9–11] perturbations proportional to the deviation from the fixed point are applied. To allow time for the system to relax to the unstable manifold, the perturbations are applied for only half the oscillatory cycle. The tracking algorithm maintains the local stability of the periodic orbit by determining the proportionality constant K_0 and the Floquet multiplier λ for each new value of the bifurcation parameter L. The amplitude of the period-1 orbit changes as the value of L is increased, and a corresponding shift of the fixed point occurs in the map. The position of the fixed point must therefore be redetermined (according to the method described in Ref. 5) for each new value of L.

Figure 8(a) shows an enlargement of Fig. 5 near the first period-doubling bifurcation at $L=18.07$. The locus of the period-1 orbit determined by the tracking algorithm is shown by the open circles. Figure 8(b) shows the Floquet multiplier λ of the period-1 orbit as a function of L. The tracking algorithm determines the Floquet multiplier of the stable as well as the unstable orbits, since, like the stability of the steady state, the stability of the orbit can be varied by varying the value of K. A symmetry breaking bifurcation, where $\lambda=1.0$, occurs at $L=18.0$, and the algorithm switches to one of the new stable solutions. At $L=18.07$, the period-doubling bifurcation takes place with $\lambda=-1.0$. The unstable period-1 orbit is then tracked through the period-doubling cascade and into the chaotic regime.

V. TRACKING STEADY FRONTS IN THE PDE SYSTEM

Equations (1) and (2) provide a more realistic description of premixed flames than the Kuramoto–Sivashinsky equation. To simulate 2-D flame fronts undergoing thermodiffusive instabilities, parameter values satisfying Eq. (11) were used in the numerical integration of Eqs. (8) and (9). The parameter values $\mathscr{L}=0.8$, $\epsilon=0.15$, and $N=20$ were chosen to reflect actual values in an experimental system.[15]

Downloaded 09 Jul 2002 to 141.14.151.181. Redistribution subject to AIP license or copyright, see http://ojps.aip.org/jcpo/jcpcr.jsp

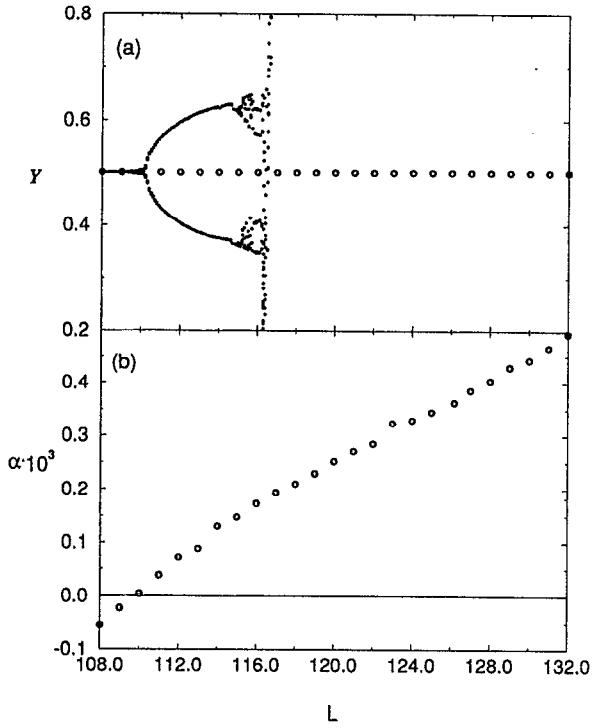

FIG. 9. Stabilization and tracking of the steady front calculated from Eqs. (8) and (9). (a) Bifurcation diagram of the front oscillations, where the solid points show the oscillation extrema of the local minimum in the front profile, $Y=(y_{\min}/L)$. The stabilized stationary state is shown by the open circles. (b) The real part of the complex conjugate eigenvalues as a function of L. Conditions are the same as in Fig. 1.

The integration yields a two-cell front over a reaction zone width ranging from $L=106$ to 116.2. As with the Kuramoto–Sivashinsky system, the behavior was characterized by monitoring the local minimum of the front contour, $Y=y_{\min}/L$. The bifurcation diagram of the autonomous system is shown in Fig. 9(a) by points representing the extrema in Y as a function of L. The behavior is qualitatively the same as that exhibited by the Kuramoto–Sivashinsky equation. The two-cell front loses stability through a Hopf bifurcation at $L=110.2$, which is followed by a symmetry breaking bifurcation at $L=114.6$. At $L=114.9$, a period-doubling cascade is initiated that gives rise to a strange attractor at $L=115.2$. This attractor coexists with another, mirror-image attractor that arises from the symmetry-breaking bifurcation. At $L=116.2$, both of these attractors are destroyed and the oscillatory behavior is replaced by an attractor with randomly appearing and disappearing minima in the front profile. The dynamical behavior governed by the new attractor is clearly more complex than the chaos arising from the period-doubling cascade.

The application of the tracking algorithm to stabilize the steady two-cell front is shown in Fig. 9. The minimum in the front contour at $Y=0.5$ is shown in Fig. 9(a) by the open circles. The steady front was stabilized from where it loses stability at the Hopf bifurcation to a value of L far beyond where the low-dimensional chaos gives way to the complex nonoscillatory behavior. The real part of the complex conjugate eigenvalues for the focus steady state is shown by the circles in Fig. 9(b); the line at $\alpha=0.0$ separates the regions of stable and unstable behavior. A control parameter analogous to that used for the Kuramoto–Sivashinsky equation was chosen to stabilize the steady front. The fuel flux at one of the boundaries was varied in proportion to z_i in Eq. (23) by varying the no-flux boundary condition around zero at one boundary grid point upstream from the front. The algorithm was initiated at $L=108.0$, where the steady state is still stable, and continuously applied to $L=132.0$.

Because the perturbations applied by the tracking algorithm become very small after the steady state is targeted, the position of the steady state is unaffected even though its stability is altered. The presence of noise and experimental errors, however, may affect both the position and stability of the steady state. During control, these fluctuations are multiplied by a factor of $\exp(\alpha T_p)$, where T_p is the period of oscillation, and can cause the algorithm to fail when αT_p is large.[10] The stabilization of the two-cell front eventually fails as L is increased, since, as shown in Fig. 9(b), the state becomes highly unstable at large L.

VI. CONCLUSION

Stabilization and tracking methods represent powerful tools for investigating the bifurcation structures of dynamical systems. Studies of dynamical systems typically rely on time series analysis, with the character of the bifurcations inferred from the qualitative changes in behavior as a system constraint is systematically varied. Information about the position and stability of unstable states has been accessible only from the application of continuation methods[23] to model descriptions. This information is necessarily dependent on the accuracy of the model. Tracking methods, on the other hand, provide information that is primary in nature and not dependent on a particular model interpretation. These methods therefore provide an expansion of the repertoire of techniques for the *experimental* characterization of dynamical systems. The development of model descriptions is thereby enhanced by the larger experimental data base for comparisons between experiment and theory.

Several different schemes have been proposed for tracking unstable states, most of which have stabilization routines based on reductions of the OGY method.[12,13] We have relied on the map-based stabilization algorithm,[9–11] since a linear stability analysis subroutine can be readily incorporated into the tracking procedure.[5] In the application presented here, modifications incorporating a phase shift allow the algorithm to be applied to focus-type stationary states. Methods based on targeting stable manifolds in phase space could also be adapted to this type of tracking scheme.

The tracking of steady and oscillatory flame fronts considered in this study points to an obvious application of such algorithms: the stabilization of desired dynamical behavior under extreme or varying conditions. Extending the regime of stable burning, for example, could serve to enhance the efficiency of combustion processes. In order to facilitate our study of stabilization and tracking, we have considered only the simplest model systems. The model independent nature

Downloaded 09 Jul 2002 to 141.14.151.181. Redistribution subject to AIP license or copyright, see http://ojps.aip.org/jcpo/jcpcr.jsp

of the method, however, suggests that more complicated flame systems, such as those subject to hydrodynamic instabilities, might also be amenable to stabilization and tracking.

Although full knowledge of the system dynamics was available in this study, the control and tracking procedure utilized only a single "experimental" observable, the position of the local minimum in the front profile. The Kuramoto–Sivashinsky equation, as well as the complete reaction–diffusion system, served as test systems for the tracking algorithm, with unstable steady states and periodic orbits stabilized and tracked through period-doubling cascades, simple period-doubling chaos, and more complex spatiotemporal chaos. Since the algorithm stabilizes states that are representative of the autonomous system, it provides a model-independent, path-following method for the investigation of experimental dynamical behavior. The stabilization of steady and oscillatory flame fronts in premixed flames is only one potential application of the algorithm; other applications should be possible in biological and chemical spatiotemporal systems.

ACKNOWLEDGMENTS

K. S. is grateful to Professor Grégoire Nicolis for his hospitality at the Service de Chimie Physique, Université Libre de Bruxelles where this manuscript was prepared. We thank the National Science Foundation (Grant No. CHE-9222616), WV-EPSCoR (Grant No. OSR-9255224), and the National Research Center For Coal and Energy for supporting this research. Acknowledgment is made to the donors of The Petroleum Research Fund, administered by the American Chemical Society, for partial support of this research.

[1] G. H. Markstein, J. Aeronaut. Sci. **3**, 18 (1951).
[2] A. G. Merzhanov and B. I. Khaikin, Prog. Energy Combust. Sci. **14**, 1 (1988).
[3] J. F. Clarke, Prog. Energy Combust. Sci. **15**, 241 (1989).
[4] G. I. Sivashinsky, Annu. Rev. Fluid Mech. **15**, 179 (1983).
[5] V. Petrov, M. F. Crowley, and K. Showalter, Phys. Rev. Lett. **72**, 2955 (1994).
[6] Z. Gills, C. Iwata, R. Roy, I. B. Schwartz, and I. Triandaf, Phys. Rev. Lett. **69**, 3169 (1992).
[7] S. Bielawski, M. Bouazaoui, D. Derozeir, and P. Glorieux, Phys. Rev. A **47**, 3276 (1994).
[8] A. Hjelmfelt and J. Ross, J. Phys. Chem. **94**, 1176 (1994).
[9] B. Peng, V. Petrov, and K. Showalter, J. Phys. Chem. **95**, 4957 (1991).
[10] V. Petrov, B. Peng, and K. Showalter, J. Chem. Phys. **96**, 7506 (1992).
[11] V. Petrov, V. Gáspár, J. Masere, and K. Showalter, Nature **361**, 240 (1993).
[12] E. Ott, C. Grebogi, and J. A. Yorke, Phys. Rev. Lett. **64**, 1196 (1990).
[13] T. Shinbrot, C. Grebogi, E. Ott, and J. A. Yorke, Nature **363**, 411 (1993).
[14] W. H. Press, B. P. Flannery, S. A. Teukolsky, and W. T. Vetterling, *Numerical Recipes* (Cambridge U. P., New York, 1986), p. 660.
[15] G. I. Sivashinsky, Combust. Sci. Technol. **15**, 137 (1977).
[16] G. I. Sivashinsky, Acta. Astronaut. **4**, 1177 (1977).
[17] Y. Kuramoto, Prog. Theor. Phys. **63**, 1885 (1980).
[18] J. M. Hyman, B. Nicolaenko, and S. Zaleski, Physica D **23**, 265 (1986).
[19] E. R. Hunt, Phys. Rev. Lett. **67**, 1953 (1991).
[20] R. Roy, T. W. Murphy, T. D. Maier, Z. Gills, and E. R. Hunt, Phys. Rev. Lett. **68**, 1259 (1992).
[21] R. W. Rollins, P. Parmananda, and P. Sherard, Phys. Rev. E **47**, R780 (1993).
[22] K. Kaneko, Prog. Theor. Phys. **69**, 1427 (1983).
[23] E. J. Doedel, Congress Num. **30**, 265 (1981); E. J. Doedel and J. P. Kernevez, *AUTO: Software for Continuation and Bifurcation Problems in Ordinary Differential Equations* (Applied Mathematics, California Institute of Technology, Pasadena, 1986).

Downloaded 09 Jul 2002 to 141.14.151.181. Redistribution subject to AIP license or copyright, see http://ojps.aip.org/jcpo/jcpcr.jsp